J. Phys. Chem. B **2010,** *114,* 8156–8165

How do Physical−Chemical Parameters Influence the Catalytic Hydrogenation of 1,3-Cyclohexadiene in Ionic Liquids?

Paul S. Campbell,[†] Ajda Podgoršek,[‡] Thibaut Gutel,[†] Catherine C. Santini,*[,†] Agílio A. H. Pádua,[‡,§] Margarida F. Costa Gomes,*[,‡,§] François Bayard,[†] Bernard Fenet,[||] and Yves Chauvin[†]

Université de Lyon Institut de Chimie de Lyon, UMR 5265 CNRS-Université de Lyon 1-ESCPE Lyon, C2P2, Equipe Chimie Organométallique de Surface, ESCPE 43 Boulevard du 11 Novembre 1918, F-69616 Villeurbanne, France, Laboratoire de Thermodynamique et Interactions Moléculaires, CNRS, UMR 6272 24 Avenue des Landais, 63177 Aubière, France, Clermont Université and Université Blaise Pascal, Clermont-Ferrand, France, and Centre Commun de RMN, UCB Lyon 1 - ESCPE Lyon, 43 Boulevard du 11 Novembre 1918, F-69626 Villeurbanne Cedex, France

Received: April 1, 2010; Revised Manuscript Received: May 11, 2010

The catalytic hydrogenation of 1,3-cyclohexadiene using $[Rh(COD)(PPh_3)_2]NTf_2$ (COD = 1,5-cyclooctadiene) was performed in two ionic liquids: 1-butyl-3-methylimidazolium bis(trifluoromethylsulfonyl)imide, $[C_1C_4Im][NTf_2]$, and 1-butyl-2,3-dimethylimidazolium bis(trifluoromethylsulfonyl)imide, $[C_1C_1C_4Im][NTf_2]$. It is observed that the reaction is twice as fast in $[C_1C_4Im][NTf_2]$ than in $[C_1C_1C_4Im][NTf_2]$. To explain the difference in reactivity, molecular interactions and the microscopic structure of ionic liquid +1,3-cyclohexadiene mixtures were studied by NMR and titration calorimetry experiments, and by molecular simulation in the liquid phase. Diffusivity and viscosity measurements allowed the characterization of mass transport in the reaction media. We could conclude that the diffusivity of 1,3-cyclohexadiene is 1.9 times higher in $[C_1C_4Im][NTf_2]$ than in $[C_1C_1C_4Im][NTf_2]$ and that this difference could explain the lower reactivity observed in $[C_1C_1C_4Im][NTf_2]$.

1. Introduction

The application of ionic liquids (ILs) in catalyzed reactions is of increasing importance,[1,2] in particular, they provide excellent media for conducting catalytic hydrogenations.[1−3] Several research groups report differences in the rates and selectivities in ILs when compared to corresponding reactions in molecular solvents.[2]

As reaction media, ILs have specific properties that may have consequences on the catalytic process. In some catalytic reactions, the difference between the use of ILs and traditional solvents has been related to the chemical role of ILs, which can serve as new ligands for the catalytic metal center, as catalyst activators, as cocatalysts, or even as catalysts themselves.[1,4,5] In other cases, differences in reactivity have a physical-chemical origin,[1,6] resulting from peculiar solvation phenomena including specific interactions between the IL and the substrate (H-bonds, cation−π),[7−9] mass transfer factors (viscosity, diffusivity),[1] and effects attributed to the highly structured nature of ILs.[10−12]

ILs have a high degree of self-organization due to the coexistence of charged moieties and hydrophobic alkyl chains, to the importance of both Coulombic and van der Waals interactions, and frequently to the presence of hydrogen bonds between the cation and the anion. In butylimidazolium ionic liquids, the alkyl side chain is sufficiently long to allow the formation of nonpolar domains that coexist with an ionic network.[13] This heterogeneous structure influences the way solutes are solvated in the ionic liquid:[14] nonpolar species will be solvated within the hydrophobic domains whereas polar substrates tend to interact with the polar network. The strength of cation−anion association[15] can also influence the possibility of establishing ion−solute specific interactions (e.g., π−cation interactions), as has been shown in the case of toluene.[9] For a nonaromatic π-system, such as 1,3-cyclohexadiene, solvation is probably a combination of more subtle interactions with the ionic liquid. This information can be assessed through the study of the thermodynamic properties of solution (solubility, enthalpy of solution) and from the characterization of the mass transfer through viscosity and diffusivity data.

The aim of this work is to study the influence of the nature of the ionic liquid on the catalytic hydrogenation of 1,3-cyclohexadiene (CYD) with $[Rh(COD)(PPh_3)_2]NTf_2$ (COD = 1,5-cyclooctadiene). First, we have quantified the difference in reactivity when the reaction is performed in two ionic liquids: 1-butyl-3-methylimidazolium bis(trifluoromethylsulfonyl)imide, $[C_1C_4Im][NTf_2]$, and 1-butyl-2,3-dimethylimidazolium bis(trifluoromethylsulfonyl)imide, $[C_1C_1C_4Im][NTf_2]$. Following this, we have attempted to rationalize the differences encountered through NMR characterization of the molecular interactions between the ionic liquids and the substrate, the study of the microscopic structure of the IL-substrate mixtures, the measurement of the thermodynamic properties of mixing (such as the solubility and the heat of mixing), the determination of the viscosity of the reaction media, and the measurement of diffusivity of CYD in the ionic liquids.

2. Experimental Section

Materials. 1-Methylimidazole (>99%, Aldrich) and 1,2-dimethylimidazole (>98%, Aldrich) were distilled prior to use.

---

* To whom correspondence should be addressed. E-mail: C.C.S., santini@cpe.fr; M.F.C.G., margarida.costa-gomes@univ-bpclermont.fr.

[†] Université de Lyon.

[‡] CNRS.

[§] Clermont Université and Université Blaise Pascal.

[||] Centre Commun de RMN.

10.1021/jp102941n

Anhydrous 1,3-cyclohexadiene (99.8%, Aldrich) and 1,3-cyclohexadiene stabilized (96%, Acros Organics, stabilized with 50 ppm of 2,6-di-*tert*-butyl-4-methylphenol, BHT) distilled over NaK alloy and stored on zeolites were used for the reaction and the physical chemical measurements, respectively. Bis(trifluoromethanesulfonyl)imide lithium salt (>99%, Solvionic) and $[Rh(COD)Cl]_2$ (>99%, Strem) were used without further purification. All other reagents and solvents were commercially available and were used as received. Ionic liquids, synthesized as previously reported,[16] were dried overnight under high vacuum and stored in a glovebox (Jacomex) to guarantee rigorously anhydrous products.

Synthesis of the Catalysts. ***[Rh(COD)(PPh₃)₂]NTf₂.*** The procedure followed was adapted from the literature.[17] A mixture of $[Rh(COD)Cl]_2$ (100 mg, 0.2 mmol) dissolved in 2 mL of dichloromethane and of $LiNTf_2$ (107 mg, 0.37 mmol) dissolved in 2 mL of water was stirred vigorously while triphenylphosphine (405 mg, 1.5 mmol) was added. After 2 h, the dichloromethane layer was removed, washed three times with 2 mL of water and dried over anhydrous Na_2SO_4. Ethanol (1 mL) and diethyl ether (2 mL) were slowly added to complete crystallization. The orange crystals were filtered off and dried under reduced pressure. Yield: 200 mg (99%). ^1H NMR (300 MHz, CD_2Cl_2): $\delta = 2.2$ (m, 8H), 4.6 (s, 4H), 7.5 (m, 30H). ^{31}P NMR (121 MHz, CD_2Cl_2): $\delta = 23.6$ with $J_{Rh-P} = 147$ Hz. ^{103}Rh NMR (500 MHz, CD_2Cl_2): $\delta = -80$ ppm with $J_{Rh-P} = 147$ Hz. Mass spectrometry: positive mode: $m/z = 473 \Rightarrow Rh(COD)(PPh_3)^+$; $627 \Rightarrow Rh(PPh_3)_2^+$. UV−vis spectroscopy (6.6 mg of $[Rh(COD)(PPh_3)_2]NTf_2$ dissolved in 2 mL of one of ionic liquids, $[C_1C_4Im][NTf_2]$ or $[C_1C_1C_4Im][NTf_2]$); spectrum recorded at $\lambda_{max} = 450$ nm.

[Rh(CYD)(PPh₃)₂]NTf₂. $[Rh(COD)(PPh_3)_2]NTf_2$ (100 mg, 9.84×10^{-5} mol) was dissolved in 1 mL of CYD. After 10 min, the excess of solvent was removed under reduced pressure. Yield: 100 mg (99%). ^1H NMR (300 MHz, CD_2Cl_2): $\delta = 2.1$ (s, 2H), 5.3 (s, 2H), 7.5 (m, 30H). ^{31}P NMR (121 MHz, CD_2Cl_2): $\delta = 25.2$ ppm with $J_{Rh-P} = 17$ Hz. Mass spectrometry: positive mode: $m/z = 707 \Rightarrow Rh(cyclohexadiene)(PPh_3)_2^+$; $m/z = 627 \Rightarrow Rh(PPh_3)_2^+$. UV−vis spectroscopy (6.6 mg of $[Rh(CYD)(PPh_3)_2]NTf_2$ dissolved in 2 mL of one of ionic liquids, $[C_1C_4Im][NTf_2]$ or $[C_1C_1C_4Im][NTf_2]$); spectrum recorded at $\lambda_{max} = 500$ nm.

Ligand Exchange. In $[Rh(CYD)(PPh_3)_2]NTf_2$ was followed by UV−vis spectroscopy. CYD (0.15 mL, 1.6 mmol) was added to a system of $[Rh(COD)(PPh_3)_2]NTf_2$ (1.6 mg, 1.6 μmol) in one of the ionic liquids, $[C_1C_4Im][NTf_2]$ or $[C_1C_1C_4Im][NTf_2]$ (1 mL). The UV−visible spectra of 1 mL of the solution were recorded on the Perkin-Elmer LAMBDA 950 Spectrophotometer in stirred and closed UV cells at $\lambda_{max} = 500$ nm every second.

Reaction with H₂. $[Rh(CYD)(PPh_3)_2]NTf_2$ (8 mg, 8.1×10^{-6} mmol) was dissolved in one of the ionic liquids, $[C_1C_4Im][NTf_2]$ or $[C_1C_1C_4Im][NTf_2]$ (5 mL) and pressurized under 1.2 bar of hydrogen. The UV−visible spectra of 1 mL of the solution were recorded at a given time at $\lambda_{max} = 500$ nm.

Hydrogenation of 1,3-Cyclohexadiene. The hydrogenation of CYD was carried out at 1.2 atm of H_2 and 30 °C. CYD (0.15 mL, 1.6 mmol) was dissolved in a system of $[Rh(COD)(PPh_3)_2]NTf_2$ (3.2 mg, 3.2 μmol) in one of ionic liquids, $[C_1C_4Im][NTf_2]$ or $[C_1C_1C_4Im][NTf_2]$ (1 mL), under argon resulting in red homogeneous solutions. The reaction mixture was kept under a hydrogen atmosphere (1.2 atm, constant pressure) until 4 mL of acetonitrile was added to the catalytic solution. The product distribution in the reaction mixture and the conversion were determined by GC analyses in presence of toluene as an internal standard. A HP6890 chromatograph equipped with FID detector and an Al_2O_3/KCl column ($L = 50$ m, $\phi_{int} = 0.32$ mm, film thickness = 5 μm) was used. The injector and detector temperatures were set to 230 °C. Samples were injected in a volume of 1 μL. The temperature of the column was fixed at 190 °C (see Supporting Information for calculations).

Solubility and Phase Diagrams. Liquid−liquid phase equilibria of the mixture of $[C_1C_4ImNTf_2]$ or $[C_1C_1C_4Im][NTf_2]$ and CYD at atmospheric pressure were determined using a dynamic method with visual detection of solution turbidity, as already described.[18]

The mixtures of ionic liquid and CYD at different compositions were prepared gravimetrically in a glass vial equipped with a stirring bar. First, the ionic liquid was introduced into a glass vial, then the appropriate amount of CYD was added and the vial was sealed. To minimize the volume of the vapor phase in equilibrium with the ionic liquid solution and to reduce the error in composition due to differential evaporation, the glass vial was almost completely filled with the mixture. The uncertainty of the mole fraction is estimated as ±0.0001. The cells were then immersed in a thermostatic water bath whose temperature was monitored using a platinum resistance thermometer with a precision of ±0.1 K. The temperature of the bath was first increased slowly until one phase was observed. The clear homogeneous system was then cooled very slowly (5 K/h) under continuous stirring. The temperature at which the first sign of turbidity (first cloudiness) appeared was considered as the temperature of the liquid−liquid phase transition. The overall accuracy in the measurement of cloud-point temperatures is estimated to be ±2 K.

Isothermal Titration Calorimetry. The heat effects resulting from mixing aliquots of CYD with the ionic liquid were measured at 303.15 K using an isothermal titration nanocalorimeter equipped with 4 mL glass cells in a Thermal Activity Monitor TAM III from TA Instruments. An electrical calibration was done before each experiment, and the instrument was chemically calibrated 5 times by titration of a 0.01 M aqueous solution of 18-crown-6 ethers with an 0.2 M aqueous solution of $BaCl_2$. The enthalpies of binding of Ba^{2+} ions to 18-crown-6 were found to be slightly higher than those reported in the literature, 2.5%[19] and 1.6%,[20,21] respectively. No correction attributable to these differences was introduced in the raw data.

Approximately 2.75 mL of degassed ionic liquid were introduced into 4 mL glass measuring and reference cells. The liquid in the measuring cell was stirred by a turbine stirrer at 160 rpm and volumes of 4 μL of CYD were injected during 180 s using a motor driven pump (Thermometric 3810 Syringe Pump) equipped with a 100 μL gastight Hamilton syringe. In all experiments, the intervals between consecutive injections were 35−40 min, which provided a good thermal stabilization of the ionic liquid solution and the return to a stable baseline. To minimize the undesirable effects of diffusion of the ionic liquid into the canula linking the CYD syringe to the cell, the canula was immersed in the sample 10 min prior the first injection.

A peak with an area proportional to the resulting heat effect Q_i translates to the thermal effect due to each injection of CYD. The integration of peaks from the recorded calorimetric plots was performed using the TAM III Assistant software. Each experiment was repeated four times to obtain reproducible values of Q_i at different concentrations within the error bar of ±2%.

Density and Viscosity. The mixtures of ionic liquid and CYD at different compositions were prepared gravimetrically following the procedure already described, including the precautions to minimize vapor headspace.[9] The viscosity of the mixture was measured at 298.15 K (controlled to within ±0.005 K and measured with the accuracy better than ±0.05 K) using a rolling ball viscometer from Anton Paar, model AMVn, equipped with capillary tubes of 3.0 and 1.8 mm in diameter. Before starting the measurements, the 3.0 mm diameter capillary tube was calibrated as a function of temperature and angle of measurement with a standard viscosity oil from Cannon (N35). The 1.8 mm diameter tube was calibrated with water by the manufacturer. The overall uncertainty of the viscosity is estimated as ±2.0%.

The densities of the mixtures, necessary to calculate the viscosities were measured in an Anton Paar vibrating tube densimeter model 512 P, at 298.15 K (measured by a calibrated PRT with an accuracy of ±0.02 K). The densimeter was calibrated using *n*-heptane, bromobenzene, and 2,4-dichlorotoluene. The overall uncertainty of the density is estimated as ±0.01%.

NMR Spectroscopy. ^{1}H, ^{13}C, and ^{31}P solution NMR data were collected at room temperature on a Bruker AC 300 MHz spectrometer with the resonance frequency at 300.130 MHz for the ^{1}H nucleus. ^{103}Rh solution NMR was carried out on a Bruker DRX 500 instrument at 298 K (nominal) with a resonance frequency at 500.130 MHz. The solvent used (CD_2Cl_2) was distilled and kept in a rotaflo with molecular sieves. Chemical shifts are reported in ppm (singlet = s, doublet = d, doublet of doublet = dd, and multiplet = m) and were measured relative to the residual proton of the solvent to $CHDCl_2$ for ^{1}H, to CD_2Cl_2 for ^{13}C, and to H_3PO_4 for ^{31}P spectra.

For ^{1}H 1D NMR spectroscopy, the samples with molar ratio $R = 0.5$ (R is the molar ratio between the amount of substance of the hydrocarbon and the amount of substance of IL) were prepared. The mixtures of ionic liquids and hydrocarbon were prepared in closed vials in a glovebox by adding the appropriate amount of CYD to each ionic liquid, $[C_1C_4Im][NTf_2]$ or $[C_1C_1C_4Im][NTf_2]$. The resulting systems were stirred for 24 h at 303 K, resulting in homogeneous monophasic solutions. Approximately 0.3 mL of the sample was then introduced into a 5 mm NMR tube. A stem coaxial capillary tube loaded with CD_2Cl_2 was inserted into the 5 mm NMR tube to avoid any contact between the deuterated solvent and the analyzed mixture. The deuterium in CD_2Cl_2 was used for the external lock of the NMR magnetic field and the residual $CHDCl_2$ in CD_2Cl_2 was used as the ^{1}H NMR external reference at 5.32 ppm. When ^{1}H NMR data are obtained in this way, the reference signal of $CHDCl_2$ remains constant and is not affected by changes in sample concentration.

For ROESY (nuclear overhauser effect spectroscopy) experiments in the rotating frame, the 2D sequence was built with the scheme proposed by Bodenhausen (the pulse sequence shown in Figure S-3 in Supporting Information).[22] The mixing time (200 ms) is split into two parts separated by a p-pulse. At each side of the spin lock the B1 field is ramped linearly (4.5 ms) to ensure adiabatic conditions for spin lock. During the first spin lock pulse, the frequency is shifted to O1 + Df whereas the second pulse frequency is set to O1 − Df; O1 is the offset frequency and Df set to give a B1 field at the magic angle. In this way, the ROESY response is roughly constant across the spectra of interest. 1D sequence PFGSE (pulse field gradient spin echo for selective excitation) has been used, and spin lock followed the same scheme as previously.

For the 2D DOSY (diffusion order spectroscopy) experiments a Bruker sequence ledbpgp2s was implemented for shorter pulse gradients to improve line shape and trapezoidal gradients (the pulse sequences shown in Figure S-6 in Supporting Information). The diffusion evolution time was 100 ms, the constant amplitude part of the gradient was 3 ms, and the cosine raising and falling part of gradient were 150 μs. The diffusion space was sampled by 32 linearly spaced gradients.

Molecular Simulation. The microscopic structures of the IL-CYD mixtures studied experimentally were also investigated by molecular simulation, using an atomistic force field that describes interactions and conformations.[23−25] CYD was represented by the optimized potential for the liquid simulations force field in its all-atom explicit version (OPLS-AA).[26] ILs were represented by a specifically parametrized force field of the OPLS-AA family in which particular attention was paid to the description of electrostatic charge distributions and torsion energy profiles. The OPLS-AA force field is known to reproduce H-bonds well; the electron density of aromatic systems is represented by the values of electrostatic charges on the relevant atoms that account for the molecular mutipoles, combined with the Lennard-Jones sites that account for dispersion interactions. Explicit polarization of electron clouds is not included in the present model. Although this may be important to correctly reproduce dynamic properties of ILs, structural features and thermodynamic quantities have been described to equivalent levels of accuracy using fixed-charge models.[27]

Molecular dynamics simulations of condensed-phase CYD−$[C_1C_4Im][NTf_2]$ and CYD−$[C_1C_1C_4Im][NTf_2]$ mixtures were performed using the DL_POLY program.[28] System sizes were chosen so as to contain about 10 000 atoms, and so the numbers of cations, anions, and CYD molecules varied according to composition (e.g., 128 ion pairs and 64 molecules of CYD for $R = 0.5$). Initial low-density configurations, with ions and molecules placed at random in periodic cubic boxes, were equilibrated to attain liquid-like densities and structures at 400 K and 1 bar. Temperature and pressure were maintained using a Nosé−Hoover thermostat and barostat, respectively. Production runs then took 500 ps with an explicit cutoff distance of 16 Å for nonbonded interactions, and long-range corrections applied for repulsive−dispersive interactions. Electrostatic energies were calculated using the Ewald summation method with a relative accuracy of 10^{-4}. Structural quantities such as radial and spatial distribution functions were calculated from configurations generated during the production runs.

3. Results and Discussion

Hydrogenation of 1,3-Cyclohexadiene. Selective hydrogenation of CYD into cyclohexene can be carried out, with good conversion rates, using Osborn's complex $[Rh(NBD)(PPh_3)_2]PF_6$ (NBD = norbornadiene) in IL media such as $[C_1C_4Im][SbF_6]$ or $[C_1C_4Im][PF_6]$.[29] To avoid impurities such as chloride and water, ILs based on the bis(trifluoromethylsulfonyl)imide anion, $[C_1C_4Im][NTf_2]$ and $[C_1C_1C_4Im][NTf_2]$, were chosen here since they are hydrophobic and liquid at room temperature and their purification is well controlled.[16] Anion exchange between the IL and the catalyst can be circumvented by replacing Osborn's complex with $[Rh(COD)(PPh_3)_2]NTf_2$ (COD = 1,5-cyclooctadiene).

In the hydrogenation experiment the appropriate quantity of CYD was added to the yellow solution of $[Rh(COD)(PPh_3)_2]NTf_2$ in $[C_1C_4Im][NTf_2]$ or $[C_1C_1C_4Im][NTf_2]$ to reach a molar ratio between CYD and IL $R = 0.5$, corresponding to a molar ratio substrate/Rh atom $r = 500$. The resulting red solution was stirred under 1.2 bar of hydrogen at 303 K. The formation of cyclohexene (CYE) was followed by GC analysis. Note that

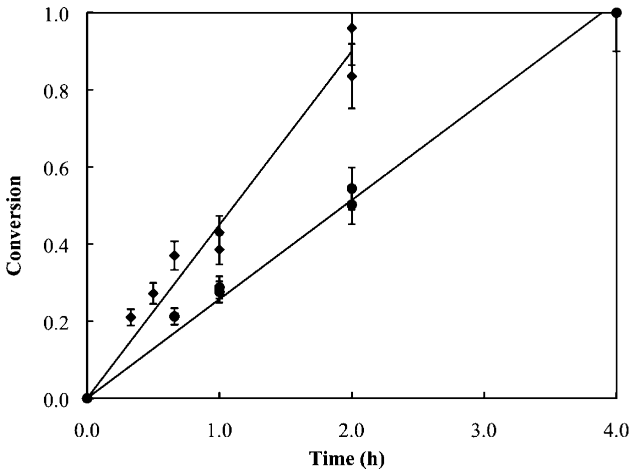

Figure 1. Hydrogenation of CYD at 303 K under 1.2 bar H_2 ($R = 0.5$ and $r = n(\text{CYD})/n(\text{Rh}) = 500$) in $[C_1C_4\text{Im}][\text{NTf}_2]$ (◆) and $[C_1C_1C_4\text{Im}][\text{NTf}_2]$ (●).

CYE is less soluble than CYD in both IL media so the system will tend to become biphasic during the course of the reaction. To avoid errors in the determination of the composition of the reaction mixture, resulting from heterogeneity of the system, the conversion was measured using GC analysis of the entire reaction system after dissolution in a mixture of acetonitrile and toluene 99:1. Each point, presented in Figure 1, corresponds to a different experiment.

As can be seen in Figure 1, hydrogenation of CYD in both ILs by $[\text{Rh(COD)(PPh}_3)_2]\text{NTf}_2$ leads quantitatively and selectively to CYE. In both cases, no significant amount (less than 2% at high or complete conversion) of cyclohexane (CYH) was detected by GC. As described in the literature, the rate of CYD reduction remains constant until near 100% conversion (1 mol of H_2 absorbed per CYD) and CYE is produced quantitatively before it is hydrogenated to CYH.[17] In $[C_1C_4\text{Im}][\text{NTf}_2]$ the conversion is complete in 2 h. This result is similar to that observed in organic solvents[17] and in other ionic liquids, such as $[C_1C_4\text{Im}][\text{PF}_6]$ or $[C_1C_4\text{Im}][\text{SbF}_6]$.[29] In $[C_1C_1C_4\text{Im}][\text{NTf}_2]$, only 50% conversion is reached after 2 h with an initial rate of hydrogenation ca. half of that in $[C_1C_4\text{Im}][\text{NTf}_2]$.

In organic solvents, during the hydrogenation of 1,3-cyclohexadiene, the catalyst first undergoes a ligand exchange, yielding $[\text{Rh(CYD)(PPh}_3)_2]^+$. This occurs more rapidly than the rate at which it then reacts with H_2.[30] The two reaction steps were investigated in both ILs. First, $[\text{Rh(CYD)(PPh}_3)_2]\text{NTf}_2$ was synthesized from $[\text{Rh(COD)(PPh}_3)_2]\text{NTf}_2$ and fully characterized. As $[\text{Rh(COD)(PPh}_3)_2]\text{NTf}_2$ is yellow ($\lambda_{\max} = 450$ nm) and $[\text{Rh(CYD)(PPh}_3)_2]\text{NTf}_2$ is red ($\lambda_{\max} = 500$ nm), the ligand exchange COD-CYD could be monitored by UV−vis spectroscopy ($\lambda = 500$ nm) in both ILs, as shown in Figure 2. This reaction is also much slower in $[C_1C_1C_4\text{Im}][\text{NTf}_2]$ than in $[C_1C_4\text{Im}][\text{NTf}_2]$.

Secondly, the red solutions of $[\text{Rh(CYD)(PPh}_3)_2]\text{NTf}_2$ in $[C_1C_4\text{Im}][\text{NTf}_2]$ or $[C_1C_1C_4\text{Im}][\text{NTf}_2]$ were exposed to hydrogen and the color disappeared with the concomitant formation of CYE. This hydrogenation reaction of CYD in $[\text{Rh(CYD)(PPh}_3)_2]\text{NTf}_2$ was also monitored by UV−vis spectroscopy in both ILs, the absorbances being represented in Figure 3. The discoloration of the medium, indicating the hydrogenation step, is also faster in $[C_1C_4\text{Im}][\text{NTf}_2]$ than in $[C_1C_1C_4\text{Im}][\text{NTf}_2]$. These results indicate that both ligand exchange and hydrogenation reactions are faster in $[C_1C_4\text{Im}][\text{NTf}_2]$. These processes, however, do not occur on the same time scale (hours versus seconds) and, as in organic solvents, ligand exchange is faster than hydrogenation. More importantly, the rate at which the CYE is produced (Figure 1) is similar to the rate of discoloration due to attack of $[\text{Rh(CYD)(PPh}_3)_2]$ by H_2 (Figure 3). Consequently, in accordance with the literature,[30] in the hydrogenation of CYD, this attack is the rate-determining step.

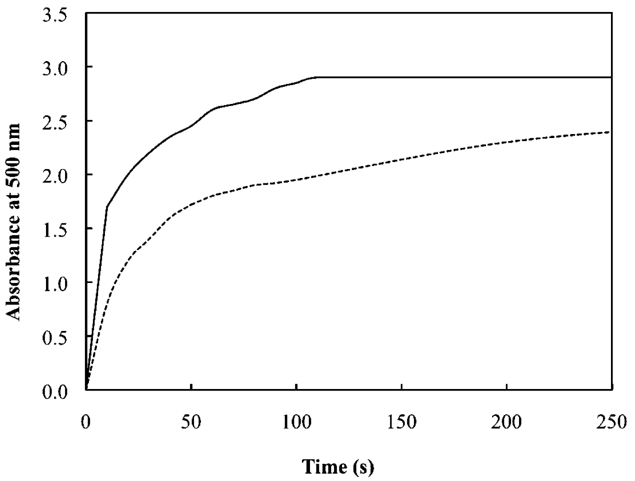

Figure 2. Evolution as a function of time of the ligand exchange reaction COD−CYD for $[\text{Rh(COD)(PPh}_3)_2]\text{NTf}_2$ in $[C_1C_4\text{Im}][\text{NTf}_2]$ (full line) and $[C_1C_1C_4\text{Im}][\text{NTf}_2]$ (dashed line) monitored at $\lambda = 500$ nm by UV−vis spectroscopy. UV−visible spectra of $[\text{Rh(COD)(PPh}_3)_2]\text{NTf}_2$ and $[\text{Rh(CYD)(PPh}_3)_2]\text{NTf}_2$ are provided in the Supporting Information (Figures S-1 and S-2).

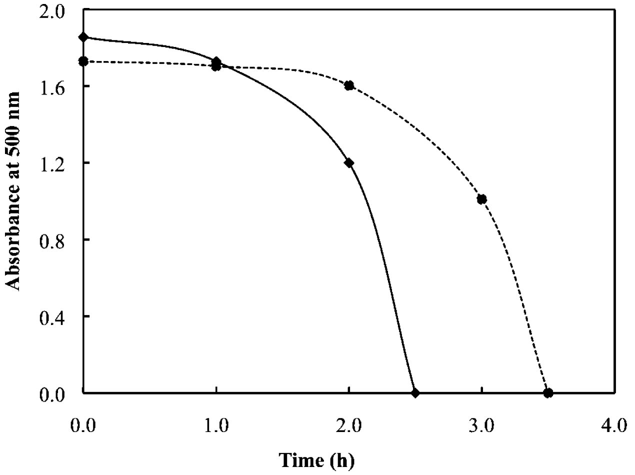

Figure 3. Evolution of the absorbance at $\lambda = 500$ nm as a function of time during the hydrogenation reaction of CYD in the presence of $[\text{Rh(CYD)(PPh}_3)_2]\text{NTf}_2$ in $[C_1C_4\text{Im}][\text{NTf}_2]$ (◆) and $[C_1C_1C_4\text{Im}][\text{NTf}_2]$ (●).

As solubilities of H_2 are similar in both ionic liquids,[31] the same overall rate of reaction would be expected. However, this is not the case and could be attributed to differences in the availability of H_2 in the different media. Indeed, even though no literature data are available for H_2 in ILs, it is generally found that the diffusion of gases is inversely dependent on the viscosity of the medium.[32] Because the same difference in the rate of reaction is noted in the ligand exchange, where H_2 is not involved, the differences in the inherent properties of each IL must be considered. For instance, studies by molecular simulations and NMR of solvation and molecular structure of similar mixtures showed that according to the nature of the IL, specific interactions with the solute differ.[7−9] In addition, mass transport factors (viscosity, diffusivity) have also been related to the

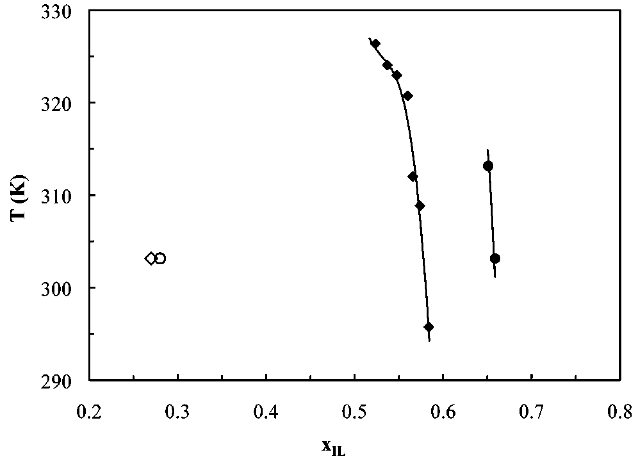

Figure 4. Liquid−liquid equilibrium diagrams for the mixture of CYD and [C_1C_4Im][NTf_2] (●) or [$C_1C_1C_4$Im][NTf_2] (◆) and solubility of toluene in [C_1C_4Im][NTf_2] (◇) or [$C_1C_1C_4$Im][NTf_2] (○).

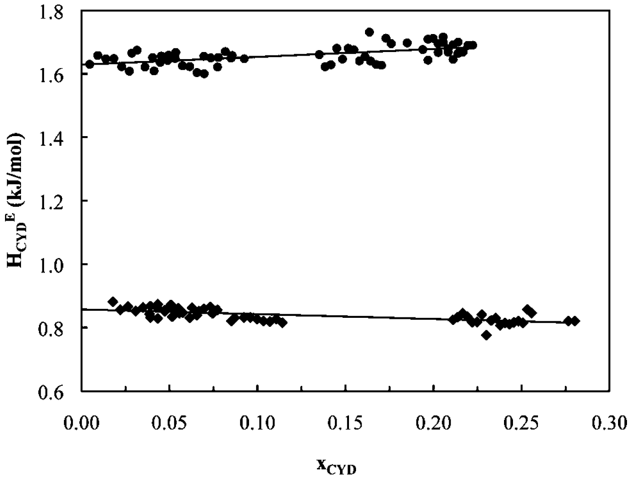

Figure 5. Partial molar excess enthalpies vs mole fraction of CYD in the binary mixture with [C_1C_4Im][NTf_2] (◆) or [$C_1C_1C_4$Im][NTf_2] (●) at 303.15 K. The lines represent functions: $H^E_{CYD} = 1.6285 + 0.2481x_{CYD}$ (●) and $H^E_{CYD} = 0.8574 - 0.1518x_{CYD}$ (◆).

reactivity[1,33] and therefore are also important parameters that we will determine and discuss here.

Solvation of 1,3-Cyclohexadiene. Figure 4 shows cloud-point temperatures as a function of composition for [C_1C_4Im][NTf_2]-CYD and [$C_1C_1C_4$Im][NTf_2]-CYD.[18,34] The observation of the cloud point with decreasing temperature was difficult, especially for the [$C_1C_1C_4$Im][NTf_2]-CYD system, because in this case the mixtures often remained in a metastable state and cloudiness persisted despite overheating. The observation of the cloud point while decreasing the temperature was not reproducible during this experiment, mainly because of the effect of precooling and kinetics of demixing, as already discussed,[33] and consequently the solubility was determined at only two temperatures. Determination of the solubility of CYD in ionic liquids by liquid−vapor equilibria measurements using a static apparatus[35,36] was not possible due to the chemical properties of CYD, such as its tendency to polymerize[37] and its compatibility with o'ring materials.

The solubility of CYD at 303.15 K, expressed in mole fraction is 0.42 in [C_1C_4Im][NTf_2] and 0.34 in [$C_1C_1C_4$Im][NTf_2] (see Figure 4), which could indicate less favorable interactions between CYD and the [$C_1C_1C_4$Im] ion in comparison with the [C_1C_4Im] ion. In the temperature range studied, both systems CYD−[C_1C_4Im][NTf_2] and CYD−[$C_1C_1C_4$Im][NTf_2] show a behavior compatible with the existence of upper critical solution temperatures and very steep liquid−liquid equilibrium lines. With this method the solubility of the ionic liquid in CYD could not be detected, as it lies below the limit of detection. From measurements and from calculations using COSMO-RS,[38] it is known that the concentration of hydrocarbons in the ionic liquid rich phase is very low, with mole fractions on the order of 10^{-4}. In comparison with aromatic molecules in these ILs, CYD is much less soluble. For instance, the solubility of toluene at 303.15 K expressed in mole fraction is 0.73 in [C_1C_4Im][NTf_2] and 0.72 in [$C_1C_1C_4$Im][NTf_2],[9] the solubility of benzene in [C_1C_4Im][NTf_2] being even higher (mole fraction of 0.78 at 303.15 K).[39] The small difference in solubility of toluene with respect to benzene can be attributed to the presence of an additional methyl group, whereas the much lower solubility of CYD is explained by less favorable interactions between the solute and the ILs. Disruption of the aromatic system changes the interactions between solute and ionic liquid and thus decreases the solubility.

The energy involved in the interactions of different solutes dissolved in ILs can be assessed by measuring the excess molar enthalpy. We have done so for both systems, CYD−[C_1C_4Im][NTf_2] and CYD−[$C_1C_1C_4$Im][NTf_2]. The excess molar enthalpy of mixing ΔH^E_{mix} was determined by isothermal titration calorimetry, from the heat effect involved in injections of small quantities of CYD into the ionic liquid, Q_{CYD}. The partial molar excess enthalpy of solute, H^E_{CYD}, was calculated according to eq 1.

$$H^E_{CYD} = \left(\frac{\partial \Delta H^E_{mix}}{\partial n_{CYD}}\right)_{n_{IL},p,T} \approx \frac{Q_{CYD}}{\Delta n_{CYD}} \qquad (1)$$

where n_{CYD} and n_{IL} denote the quantity of CYD and IL, respectively, ΔH^E_{mix} is the excess molar enthalpy of the entire system (enthalpy of mixing) and Δn_{CYD} is the quantity of solute per injection. Δn_{CYD} was calculated from the injected volumes and the density of CYD was obtained from the literature.[40] In these calculations, heat due to evaporation of the solute from IL solution is assumed to be negligible. Hence, no correction for the vapor pressure of the solute was made.

Figure 5 represents partial molar excess enthalpies of CYD in both ILs at 303.15 K as a function of composition. A larger dispersion of the values (up to 3%), especially at higher concentration, was observed. At times, before each injection of CYD into the IL, an exothermic effect was detected, mainly originating from insufficient mixing of both components at the beginning of the injection period. As already discussed in the literature[41] in the case of aromatic hydrocarbons, the rate of dissolution of nonpolar, low density and low viscosity CYD in the IL is slow and sometimes leads to formation of a solute-rich layer on the surface of the solution. This is often accompanied by partial evaporation or even polymerization of CYD before the mixing process is complete, hence disturbing the measurements. A large number of injections were made to ensure reliability. [The formation of a polymer was observed and confirmed by NMR analysis.[37] This side reaction is attributed to the fact that CYD has been distilled to eliminate the stabilizer BHT before the physical chemical measurements.]

The dependence of partial molar excess enthalpy of CYD in [C_1C_4Im][NTf_2] and [$C_1C_1C_4$Im][NTf_2] on the mole fraction was approximated by a linear regression, eq 2 and Figure 5. The partial excess molar enthalpies of CYD in both ILs at infinite dilution, $H^{E\infty}_{CYD}$, were obtained from eq 2 by setting $x_{CYD} = 0$

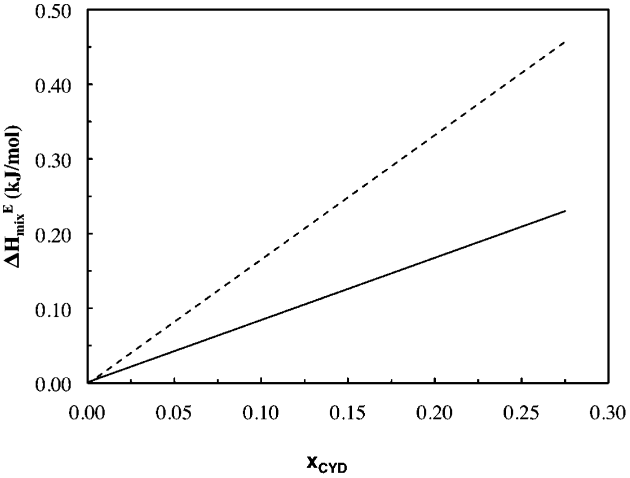

Figure 6. Excess molar enthalpies of the systems: CYD−$[C_1C_4Im][NTf_2]$ (—) and CYD−$[C_1C_1C_4Im][NTf_2]$ (---) vs the mole fraction of CYD at 303.15 K.

TABLE 1: Excess Molar Enthalpies of Mixing of Organic Solutes and Ionic Liquids at Mole Fraction of Solute 0.1

ionic liquid	solute	ΔH^E_{mix} (J/mol)	T (K)
$[C_1C_4Im][NTf_2]$	1,3-cyclohexadiene	$+85 \pm 9$	303.15
$[C_1C_1C_4Im][NTf_2]$	1,3-cyclohexadiene	$+164 \pm 10$	303.15
$[C_1C_4Im][NTf_2]$	benzene	−189.8[42]	363.15
$[C_1C_4Im][NTf_2]$	toluene	−150.4[40]	363.15
$[C_1C_4Im][NTf_2]$	methylcyclohexane	+435.6[40]	363.15
$[C_1C_2Im][NTf_2]$	benzene	−112.7[34]	323.15
$[C_1C_2Im][NTf_2]$	toluene	−115.6[39]	298.15
$[C_1C_2Im][NTf_2]$	cyclohexene	+356.5[34]	323.15
$[C_1C_2Im][NTf_2]$	cyclohexane	+394.0[34]	323.15

and were found to be 0.857 kJ mol^{-1} for CYD−$[C_1C_4Im][NTf_2]$ and 1.629 kJ mol^{-1} for CYD−$[C_1C_1C_4Im][NTf_2]$.

$$H^E_{CYD}\ (\text{kJ/mol}) = a + bx_{CYD} \qquad (2)$$

By integrating eq 1 and taking into account eq 2, we calculated the excess molar enthalpy of mixing ΔH^E_{mix} by

$$\begin{aligned}\Delta H^E_{mix}\ (\text{kJ/mol}) &= \Delta H_{mix} = \int_0^{n_{CYD}} H^E_{CYD}\, dn_{CYD}/(n_{CYD} + n_{IL}) \\ &= (a + b)x_{CYD} + b(1 - x_{CYD})\ln(1 - x_{CYD})\end{aligned} \qquad (3)$$

From Figure 6, it can be seen that the excess molar enthalpies of mixing for the binary mixtures of CYD and $[C_1C_4Im][NTf_2]$ and $[C_1C_1C_4Im][NTf_2]$ are positive over the studied range of compositions. The values of excess molar enthalpy of mixing of several aromatic and nonaromatic solutes in ILs together with our results are presented in Table 1. To the best of our knowledge the energetics of solvation of organic solutes in $[C_1C_1C_4Im][NTf_2]$ had never been studied; therefore, we could establish comparisons only for 3-alkyl-1-methylimidazolium bis(trifluoromethylsulfonyl)imide, $[C_1C_nIm][NTf_2]$. Negative values of ΔH^E_{mix} for benzene and toluene in $[C_1C_4Im][NTf_2]$ indicate more favorable interactions between aromatic systems and imidazolium ILs than for methylcyclohexane, for which the enthalpy of mixing is positive. A similar effect was observed in $[C_1C_2Im][NTf_2]$, where the aromatic solutes have more favorable interactions leading to negative enthalpies of mixing and higher solubilities. Cyclohexene, due to the presence of a double bond, also has lower enthalpy of mixing than cyclohexane in $[C_1C_2Im][NTf_2]$. As expected, the values of ΔH^E_{mix} for CYD obtained here are intermediate between the values for cyclohexene and benzene. Comparison of $[C_1C_4Im][NTf_2]$ and $[C_1C_1C_4Im][NTf_2]$ shows that introduction of an additional methyl group on the C2 carbon of the imidazolium ring strongly affects the interaction with molecules of CYD, which becomes less favorable. To rationalize the differences in the solvation of CYD in both ILs, and to complement the enthalpic data with structural information, the microscopic structure of the mixtures was investigated using NMR and molecular simulation.

Molecular Structure of the Reaction Media. The molecular structure of the mixture of CYD and ILs, $[C_1C_4Im][NTf_2]$ and $[C_1C_1C_4Im][NTf_2]$, and therefore the sites of specific interactions were studied by ^1H NMR and ROESY experiments. The ^1H NMR chemical shifts of the CYD−IL mixtures at $R = 0.5$ were not significantly different from those of the neat CYD and ILs, in both cases (Table S-1 in Supporting Information).

NOESY experiments exhibited very weak or null cross peak intensities. This was probably due to the fact that the quantity $\omega\tau c$ was such that the NOE intensity was close to the null point. Rotating frame NOE experiments (ROESY) allowed us to obtain positive NOEs irrespective of the long rotational correlation time due to the high viscosity of the system. In $^1H-^1H$ ROESY techniques based on space cross relaxations, the selective irradiation of a proton group affects the intensities of integrals of all proton groups that are spatially close but not necessarily connected by chemical bonds. The method is based on the assumption of short-range intermolecular distances (4−5 Å).[43] The strength of the ROE signal is proportional to the inverse sixth power of the distance between the atoms, $I \propto 1/r.^6$ In the liquid state, this relation is possible if the intermolecular association is tight enough to turn the intermolecular relaxation into “intramolecular” within the ion pair or ion−molecule association.[41] Highly structured, bulk ionic liquids seem to fulfill these requirements, thus allowing the use of the intermolecular ROESY to derive lower limits for interionic distances. Consequently, the intensity of the integrals (I_{CYD-IL}) could be considered as roughly inversely proportional to the intermolecular distances (Figure S-4 and S-5, Supporting Information).

Molecular mechanics calculations have been performed using the SYBYL software with the TRIPOS force field developed by Clark et al.[44] on isolated pairs of CYD and imidazolium cations. Intermolecular distances were fixed using results from NMR ROESY experiments and the energy of both systems, CYD−$[C_1C_4Im]$ and CYD−$[C_1C_1C_4Im]$, were minimized. The average distances between molecules of CYD and the imidazolium cations were determined from the geometry at the potential energy minimum. CYD is mainly located near the butyl chain of $[C_1C_4Im][NTf_2]$, the π bonds being located closer to the imidazolium cation, a configuration similar to that previously observed for toluene (Figure 7).[9]

Access to the microscopic structure of the mixtures in the condensed liquid phase is possible using molecular dynamics simulation with all atoms explicitly present and periodic boundary conditions to represent a vitually infinite system. Condensed-phase simulations take into account all the two-body interactions from the environment of each molecule or ion. The molecular simulation details are given in the Experimental Section. In Figure 8 are plotted the site−site radial distribution functions—the probability of finding pairs of atoms at a given distance, compared to the average—between the hydrogens on Cβ of CYD, Hβ, and selected atoms of the $[C_1C_4Im]$ and $[C_1C_1C_4Im]$ cations at $R = 0.5$ (atoms are labeled as indicated in Scheme 1). In both cases, there is a higher probability (a

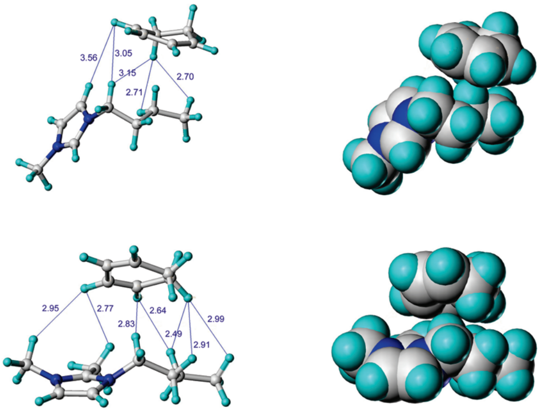

Figure 7. Representation of molecular positions in saturated solutions of CYD−[C_1C_4Im][NTf_2] and CYD−[$C_1C_1C_4$Im][NTf_2] from ROESY NMR extrapolation.

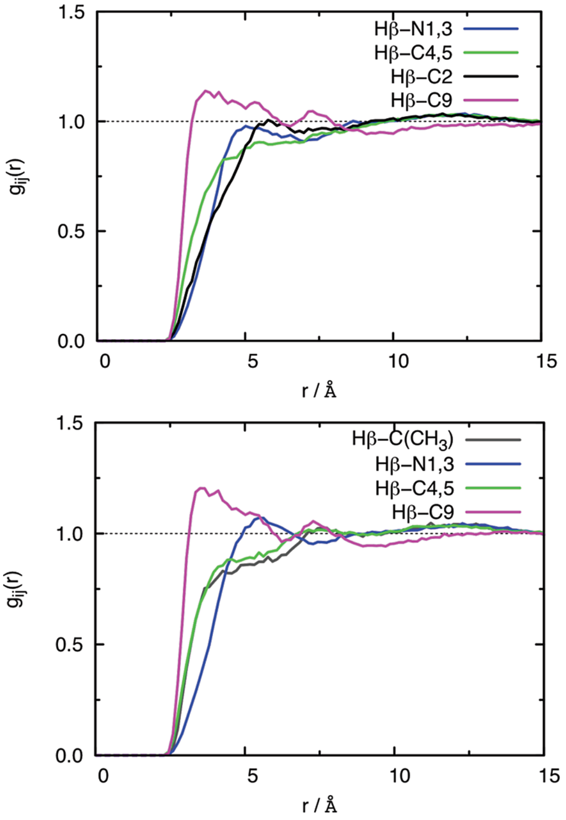

Figure 8. Radial distribution functions between hydrogen on Cβ of CYD, Hβ, and selected sites in the [C_1C_4Im] cation (top) and [$C_1C_1C_4$Im] cation (bottom), for $R = 0.5$. Atoms are labeled as indicated in Scheme 1.

stronger association) of finding all hydrogen atoms of CYD near the side chain rather than in the vicinity of the aromatic nucleus region of the imidazolium cation. This means that CYD is preferentially solvated in the nonpolar domain of the ILs, as already observed for saturated hydrocarbons and for the methyl group of toluene. This orientation effect relative to the cation is less distinct for CYD than for toluene,[9] as expected given the weaker cation−π interactions of the former.

Figure 9 represents the comparison of the radial distribution functions of the mixtures CYD−[C_1C_4Im][NTf_2] and CYD−[$C_1C_1C_4$Im][NTf_2], again at $R = 0.5$, between hydrogen on Cβ and Cα of CYD and C_2 of the imidazolium rings. It can be seen that both these hydrogen atoms are found with a higher probability closer to C_2 in [$C_1C_1C_4$Im][NTf_2] than in [C_1C_4Im][NTf_2]. The strong hydrogen bond between C2−H and the anion in [C_1C_4Im][NTf_2] prevents such an interaction with CYD. This observation is consistent with the distances between the IL cations and CYD obtained from ROESY experiments and molecular mechanics calculations on isolated pairs, as seen in Figure 7.

Detailed structural features are much better perceived in 3-dimensional spatial distribution functions. In Figure 10 is represented the distribution of ions around a CYD molecule. In blue is plotted the iso-surface corresponding to a local density of twice the average density of C_2 carbon atoms of the imidazolium cations. Cation headgroups (the blue regions) are located above and below the CYD ring, interacting preferentially with the π-system of CYD. It can be seen that the terminal carbons of the alkyl side chain, C_9 (the gray regions), surround the CYD molecule. Oxygen atoms of the NTf_2^- anion (plotted in red) are found in the plane of CYD interacting with the hydrogen atoms of the double bonds. Similar results have been previously obtained for toluene in the same ILs.[9] This shows that although in CYD the π-system is smaller than that of a fully aromatic system, it still determines the structure of the solvation shell in ILs with cations positioned above and below the plane of CYD and anion in the plane.

Figure 11 shows spatial distribution functions around the [C_1C_4Im] and the [$C_1C_1C_4$Im] cations. With both cations, CYD (the white regions) is preferentially located above and below the plane of the imidazolium ring at distances greater than those of the closest cation−anion pairs. In red is plotted the iso-surface corresponding to the local density of 4 times the average density of the oxygen atoms from NTf_2^- anions. As can be seen, for [C_1C_4Im][NTf_2] the probability of finding the oxygen of NTf_2^- near the C_2−H of the imidazolium cation is higher than the carbon of CYD, indicating a strong H-bond. The situation is completely different for [$C_1C_1C_4$Im][NTf_2], where the probability of finding the carbon of CYD near the C_2 of the cation is higher than that of the oxygen atoms of NTf_2^-. As already found in the case of solvation of toluene,[9] interactions of the [$C_1C_1C_4$Im] cation with the anion are mainly through H_4, H_5 and also the nitrogen atoms, N_1 and N_3, whereas in [C_1C_4Im] cation−anion interactions are mainly through C_2−H bonds.

Mass Transport in Reaction Media. To establish whether the difference in rate of catalytic hydrogenation of CYD can be attributed to the specific interactions or only to differences in thermophysical propreties of the reaction media, which affect the mobility of molecules, the density and viscosity of the mixtures of [C_1C_4Im][NTf_2]-CYD and [$C_1C_1C_4$Im][NTf_2]-CYD at $R = 0.5$ were measured at 298.15 K and atmospheric pressure (Table 2 and Figure S-7 in Supporting Information). The additional methyl group on the imidazolium carbon C_2 in [$C_1C_1C_4$Im][NTf_2] naturally lowers both the mass and molar density of the liquid in comparison with [C_1C_4Im][NTf_2]. On the other hand, the viscosity of pure [$C_1C_1C_4$Im][NTf_2] and also of its mixture with CYD is roughly twice that of [C_1C_4Im][NTf_2], as reported in Table 2. Diffusion coefficients (D) of CYD in both ILs at $R = 0.5$ were determined from extrapolation of DOSY data (Figure S-6 in Supporting Information): 187.5 $\mu m^2/s$ in [C_1C_4Im][NTf_2] against 97 $\mu m^2/s$ in [$C_1C_1C_4$Im][NTf_2], meaning that diffusion of CYD in [C_1C_4Im][NTf_2] is 1.9 times faster than in [$C_1C_1C_4$Im][NTf_2]. Since, according to the Stokes−Einstein relation, the diffusion coefficient is inversely proportional to the viscosity of the medium, the ratio of values of D obtained is in agreement with the ratio of measured viscosities of both mixtures at $R = 0.5$, which is η(CYD−[$C_1C_1C_4$Im][NTf_2])/η(CYD−[C_1C_4Im][NTf_2])

SCHEME 1: Atom Labeling of CYD, 1-Butyl-3-methylimidazolium, and 1-Butyl-2,3-dimethylimidazolium Cations

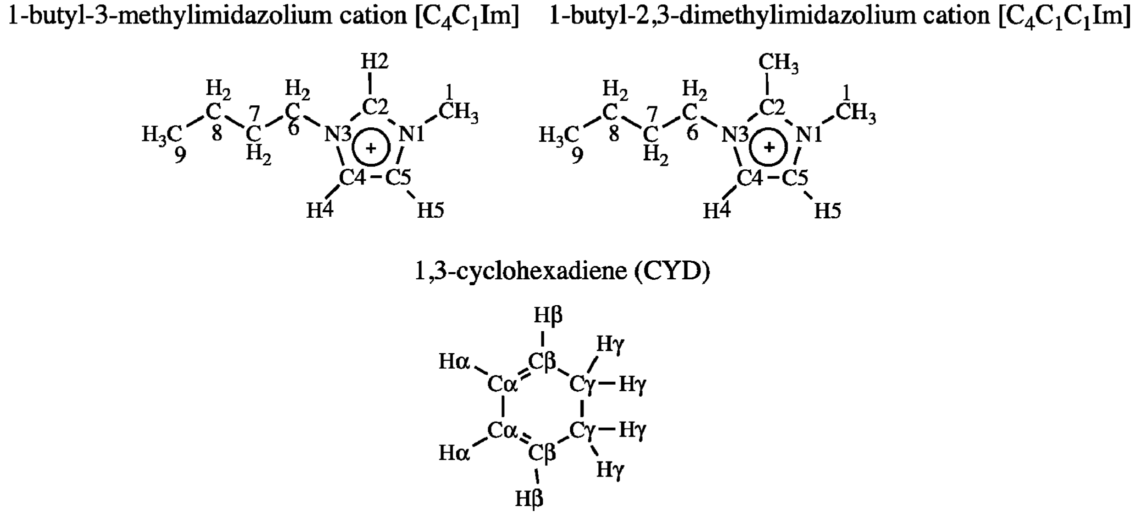

= 1.9. The availability of H_2 for the hydrogenation reaction is also dependent on the diffusivity of the gas in both ILs. No experimental data were found on the diffusivity of hydrogen in ILs, but it is expected that it will also be inversely proportional to the viscosity of the liquid medium since H_2 interacts weakly with ILs (its solubility is very low[45,46]). Molecular simulation results for the diffusivity of H_2 in $[C_6C_1Im][NTf_2]$ at different temperatures have recently been published.[47] We have calculated that the increase of diffusivity of hydrogen and the decrease in viscosity of $[C_6C_1Im][NTf_2]$ at the different temperatures[48] are comparable within the same order of magnitude. This is commensurate with the expected precision of the molecular simulation results.[27] All these results indicate that the difference in reactivity of both systems at $R = 0.5$ can be mainly assigned to the difference in viscosity and therefore in mobility of the molecules, namely, CYD in the exchange reaction and both H_2 and CYD in the hydrogenation reaction.

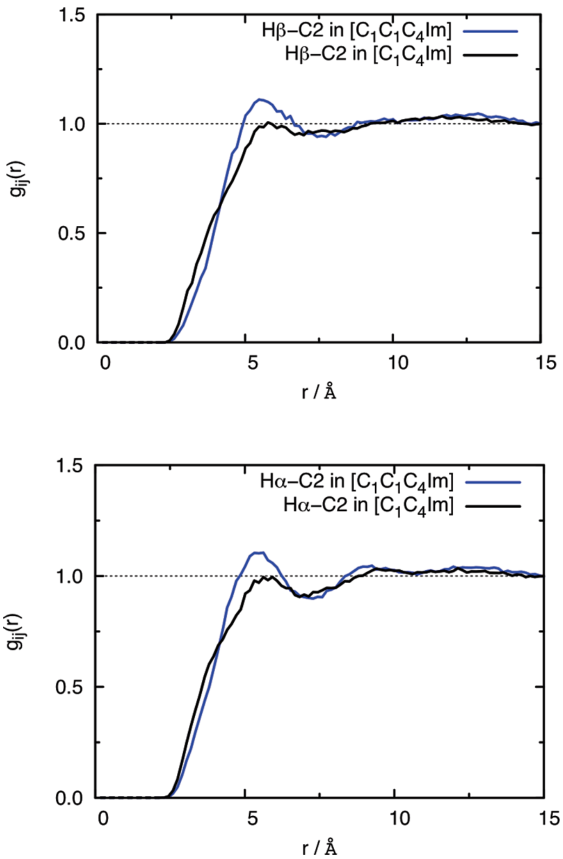

Figure 9. Comparison of site–site radial distribution functions between chosen atoms in CYD and the cations, in CYD–$[C_1C_4Im][NTf_2]$ (top) and CYD–$[C_1C_1C_4Im][NTf_2]$ (bottom) for $R = 0.5$. Atoms are labeled as indicated in Scheme 1.

4. Conclusion

In this work, we studied the impact of two ionic liquid solvents on the rates of two reaction steps of the catalytic hydrogenation of 1,3-cyclohexadiene (CYD) with $[Rh(COD)(PPh_3)_2]NTf_2$: the ligand exchange $[Rh(COD)(PPh_3)_2]NTf_2$ to $[Rh(CYD)(PPh_3)_2]NTf_2$, and the catalytic hydrogenation of CYD itself (COD = 1,5-cyclooctadiene). It was found that

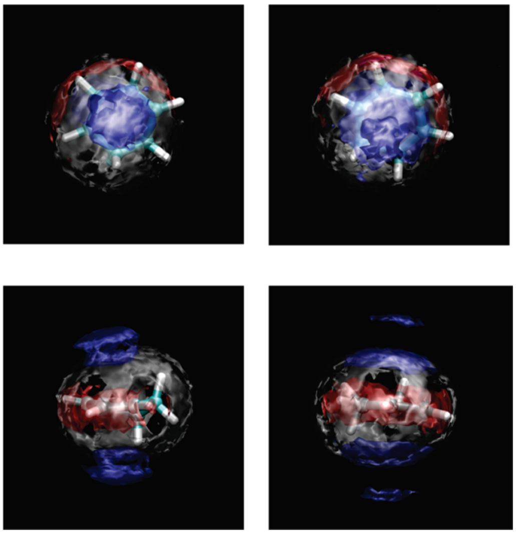

Figure 10. Spatial distribution functions around the C_2 carbon of CYD in CYD–$[C_1C_4Im][NTf_2]$ (left) and CYD–$[C_1C_1C_4Im][NTf_2]$ (right) at $R = 0.5$. In blue is plotted the iso-surface corresponding to a local density of twice the average density of the C_2 carbon of the imidazolium cations. In gray is plotted the iso-surface corresponding to a local density of twice the average density of terminal methyl carbons from the butyl side chain, C_9. In red is plotted the iso-surface corresponding to a local density of twice the average density of oxygen atoms from the NTf_2^- anion. Oxygen atoms are located in the CYD plane interacting with hydrogen atoms of double bonds, Hα and Hβ.

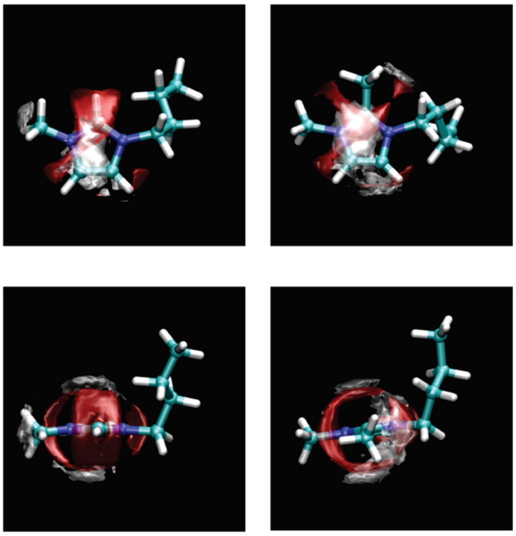

Figure 11. Spatial distribution functions around the C_2 carbon of the cations in CYD−$[C_1C_4Im][NTf_2]$ (left) and CYD−$[C_1C_1C_4Im][NTf_2]$ (right) at $R = 0.5$. Above and below are different views of the same iso-surfaces. In white is plotted the iso-surface corresponding to a local density of twice the average density of Cα of CYD. In red is plotted the iso-surface corresponding to a local density of 4 times the average density of oxygen atoms from the NTf_2^- anion.

TABLE 2: Density and Viscosity, at 298.15 K and Atmospheric Pressure, of Mixtures of CYD−$[C_1C_4Im][NTf_2]$ and CYD−$[C_1C_1C_4Im][NTf_2]$ at $R = 0.5$

x_{IL}	R	ρ (g cm^{-3})	η (mPa s)
	CYD−$[C_1C_4Im][NTf_2]$		
1.000	0.000	1.4375	48.45
0.667	0.498	1.3597	24.87
	CYD−$[C_1C_1C_4Im][NTf_2]$		
1.000	0.000	1.4177	105.00
0.662	0.510	1.3442	47.13

both steps are twice as fast in 1-butyl-3-methylimidazolium bis(trifluoromethylsulfonyl)imide, $[C_1C_4Im][NTf_2]$, than in 1-butyl-2,3-dimethylimidazolium bis(trifluoromethylsulfonyl)imide, $[C_1C_1C_4Im][NTf_2]$. The rate-determining step in both ionic liquids is the hydrogenation of CYD step.

Molecular dynamics simulations and NMR experiments indicate that in both ILs, for a molar ratio CYD/IL equal to 0.5, CYD is solvated preferentially in lipophilic regions (in close proximity to the alkyl side chains of the cations) as already observed for saturated hydrocarbons and the methyl group of toluene. In addition, in $[C_1C_1C_4Im][NTf_2]$ the probability of finding CYD near the C2 of the cation is higher than in $[C_1C_4Im][NTf_2]$, in agreement with the shorter CYD−$[C_1C_1C_4Im]$ distances determined by ROESY NMR. On the other hand, a higher solubility of CYD in $[C_1C_4Im][NTf_2]$ and smaller positive enthalpies of mixing for the CYD−$[C_1C_4Im][NTf_2]$ system in comparison with CYD−$[C_1C_1C_4Im][NTf_2]$ indicate more favorable interactions between CYD and the $[C_1C_4Im]$ cation than with the $[C_1C_1C_4Im]$ cation. These thermodynamic factors concur with the differences in catalytic activity, although they cannot fully explain the differences observed. Association between macroscopic thermodynamic information, thermophysical data, and microscopic structural information is necessary to fully explain the differences in reactivity found in both IL media.

Pure $[C_1C_1C_4Im][NTf_2]$ has a higher viscosity than pure $[C_1C_4Im][NTf_2]$, and the same relative values are observed in the mixtures with CYD. These differences in viscosity induce higher diffusion coefficients in $[C_1C_4Im][NTf_2]$ (187.5 $\mu m^2/s$) when compared to those in $[C_1C_1C_4Im][NTf_2]$ (97 $\mu m^2/s$), meaning that diffusion of CYD in $[C_1C_4Im][NTf_2]$ is 1.9 times faster than in $[C_1C_1C_4Im][NTf_2]$. Since the diffusion coefficient is inversely proportional to the viscosity of the medium, the values obtained are in agreement with the Stokes−Einstein relation, since the ratio of measured viscosities of both ionic liquids at $R = 0.5$ $\eta(\text{CYD}-[C_1C_1C_4Im][NTf_2])/\eta(\text{CYD}-[C_1C_4Im][NTf_2])$ is also 1.9. The diffusion coefficient of gases is also expected to vary inversely with the viscosity of the medium. These results indicate that the difference in the rate of both ligand exchange and hydrogenation of CYD with $[Rh(COD)(PPh_3)_2]NTf_2$ in $[C_1C_4Im][NTf_2]$ and $[C_1C_1C_4Im][NTf_2]$ can be attributed to the difference in viscosity of both ionic liquids, hence the mobility of the molecules in solution.

Acknowledgment. A.P. acknowledges the postdoctoral grant by the project ANR CALIST and P.C. acknowledges the Ph.D. grant attributed by the *Ministère de l'Enseignement Supérieur et de la Recherche*, France.

Supporting Information Available: Determination of the conversion and the composition of the reaction mixture by GC. UV−vis spectra of $[Rh(COD)(PPh_3)_2]NTf_2$ and $[Rh(CYD)(PPh_3)_2]NTf_2$, ROESY and DOSY NMR pulse sequences, ^1H NMR shifts and ROESY NMR spectra of the mixture of CYD in $[C_1C_4Im][NTf_2]$ and $[C_1C_1C_4Im][NTf_2]$. This material is available free of charge via the Internet at http://pubs.acs.org.

References and Notes

(1) Wasserscheid, P.; Welton, T. *Ionic Liquids in Synthesis*; Wiley VCH: Weinheim, Germany, 2008.

(2) Parvulescu, V. I.; Hardacre, C. *Chem. Rev.* **2007**, *107*, 2615.

(3) Dyson, P. J.; Zhao, D. Hydrogenation. *Multiphase Homogeneous Catalysis*; Wiley-VCH: Weinheim, 2005; Vol. 2, pp 494.

(4) Olivier-Bourbigou, H.; Vallee, C. *Multiphase Homogeneous Catalysis*; Wiley-VCH: Weinheim, 2005; Vol. 2, pp 413−431.

(5) Hintermair, U.; Gutel, T.; Slawin, A. M. Z.; Cole-Hamilton, D. J.; Santini, C. C.; Chauvin, Y. *J. Organomet. Chem.* **2008**, *693*, 2407.

(6) Dupont, J.; Suarez, P. A. Z. *Phys. Chem. Chem. Phys.* **2006**, *8*, 2441.

(7) Dupont, J.; Suarez, P. A. Z.; De Souza, R. F.; Burrow, R. A.; Kintzinger, J.-P. *Chem.*—*Eur. J.* **2000**, *6*, 2377.

(8) Lachwa, J.; Bento, I.; Duarte, M. T.; Canongia Lopes, J. N.; Rebelo, L. P. N. *Chem. Commun.* **2006**, 2445.

(9) Gutel, T.; Santini, C. C.; Padua, A. A. H.; Fenet, B.; Chauvin, Y.; Canongia Lopes, J. N.; Bayard, F.; Costa Gomes, M. F.; Pensado, A. S. *J. Phys. Chem. B* **2009**, *113*, 170.

(10) Mele, A.; Romano, G.; Giannone, M.; Ragg, E.; Fronza, G.; Raos, G.; Marcon, V. *Angew. Chem., Int. Ed.* **2006**, *45*, 1123.

(11) Padua, A. A. H.; Costa Gomes, M. F.; Canongia Lopes, J. N. A. *Acc. Chem. Res.* **2007**, *40*, 1087.

(12) Triolo, A.; Russina, O.; Bleif, H.-J.; Di Cola, E. *J. Phys. Chem. B* **2007**, *111*, 4641.

(13) Canongia Lopes, J. N.; Padua, A. A. H. *J. Phys. Chem. B* **2006**, *110*, 3330.

(14) Canongia Lopes, J. N.; Costa Gomes, M. F.; Padua, A. A. H. *J. Phys. Chem. B* **2006**, *110*, 16816.

(15) Hunt, P. A. *J. Phys. Chem. B* **2007**, *111*, 4844.

(16) Magna, L.; Chauvin, Y.; Niccolai, G. P.; Basset, J.-M. *Organometallics* **2003**, *22*, 4418.

(17) Schrock, R. R.; Osborn, J. A. *J. Am. Chem. Soc.* **1976**, *98*, 4450.

(18) Blesic, M.; Canongia Lopes, J. N.; Padua, A. A. H.; Shimizu, K.; Costa Gomes, M. F.; Rebelo, L. P. N. *J. Phys. Chem. B* **2009**, *113*, 7631.

(19) Izatt, R. M.; Terry, R. E.; Haymore, B. L.; Hansen, L. D.; Dalley, N. K.; Avondet, A. G.; Christensen, J. J. *J. Am. Chem. Soc.* **1976**, *98*, 7620.

(20) Liu, Y. F.; Sturtevant, J. M. *Protein Sci.* **1995**, *4*, 2559.

(21) Briggner, L. E.; Wadso, I. *J. Biochem. Biophys. Methods* **1991**, *22*, 101–118.

(22) Cutting, B.; Ghose, R.; Bodenhausen, G. *J. Magn. Reson.* **1999**, *138*, 326.

(23) Canongia Lopes, J. N.; Deschamps, J.; Padua, A. A. H. *J. Phys. Chem. B* **2004**, *108*, 2038.

(24) Canongia Lopes, J. N.; Padua, A. A. H. *J. Phys. Chem. B* **2004**, *108*, 16893.

(25) Canongia Lopes, J. N.; Shimizu, K.; Padua, A. A. H.; Umebayashi, Y.; Fukuda, S.; Fujii, K.; Ishiguro, S. I. *J. Phys. Chem. B* **2008**, *112*, 9449.

(26) Jorgensen, W. L.; Maxwell, D. S.; Tirado-Rives, J. *J. Am. Chem. Soc.* **1996**, *118*, 11225.

(27) Maginn, E. J. *Acc. Chem. Res.* **2007**, *40*, 1200.

(28) Smith, W.; Forester, T. R.; Todorov, I. T.; *The DL_POLY molecular simulation package*, 2.20 ed.; T. D. P. m. s., Ed.; STFC Daresbury Laboratorys, Warrington, U.K., 2007.

(29) Chauvin, Y.; Mussmann, L.; Olivier, H. *Angew. Chem., Int. Ed.* **1996**, *34*, 2698.

(30) Schrock, R. R.; Osborn, J. A. *J. Am. Chem. Soc.* **1976**, *98*, 2134.

(31) Costa Gomes, M. F. Unpublished results.

(32) Camper, D.; Becker, C.; Koval, C.; Noble, R. *Ind. Eng. Chem. Res.* **2006**, *45*, 445.

(33) Cui, Y.; Biondi, I.; Chaubey, M.; Yang, X.; Fei, Z.; Scopelliti, R.; Hartinger, C. G.; Li, Y.; Chiappe, C.; Dyson, P. J. *Phys. Chem. Chem. Phys.* **2010**, *12*, 1834.

(34) Domañska, U.; Żołek-Tryznowska, Z.; Królikowski, M. *J. Chem. Eng. Data* **2007**, *52*, 1872.

(35) Kato, R.; Krummen, M.; Gmehling, J. *Fluid Phase Equilib.* **2004**, *224*, 47.

(36) Husson, P.; Pison, L.; Jacquemin, J.; Costa Gomes, M. F. *Fluid Phase Equilib.* **2010**, DOI: 10.1016/j.fluid.2010.02.021.

(37) Natori, I.; Imaizumi, K.; Yamagishi, H.; Kazunori, M. *J. Polym. Sci., Part B* **1998**, *36*, 1657.

(38) Domanska, U.; Pobudkowska, A.; Eckert, F. *Green Chem.* **2006**, *8*, 268.

(39) Lachwa, J.; Bento, I.; Duarte, M. T.; Canongia Lopes, J. N.; Rebelo, L. P. N. *Chem. Commun.* **2006**, 2445.

(40) Letcher, T. M.; Marsicano, F. *J. Chem. Thermodyn.* **1974**, *6*, 509.

(41) Marczak, W.; Verevkin, S. P.; Heintz, A. *J. Solution Chem.* **2003**, *32*, 519.

(42) Nebig, S.; Bolts, R.; Gmehling, J. *Fluid Phase Equilib.* **2007**, *258*, 168.

(43) Frezzato, D.; Rastrelli, F.; Bagno, A. *J. Phys. Chem.B* **2006**, *110*, 5676.

(44) Clark, M.; Cramer, R. D., III; Van Opdenbosch, N. *J. Comput. Chem.* **1989**, *10*, 982–1012. Sybil program version 7.0, Tripos Inc., 1699 South Hanley Rd., St. Louis, MO 63144, U.S.A.

(45) Jacquemin, J.; Costa Gomes, M. F.; Husson, P.; Majer, V. *J. Chem. Thermodyn.* **2006**, *38*, 490. Jacquemin, J.; Husson, P.; Majer, V.; Costa Gomes, M. F. *Fluid Phase Equilib.* **2006**, *240*, 87.

(46) Costa Gomes, M. F. *J. Chem. Eng. Data* **2007**, *52*, 472.

(47) Shi, W.; Sorescu, D. C.; Luebke, D. R.; Keller, M. J.; Wickramanyake, S. *J. Phys. Chem. B* **2010**, *114*, 6431.

(48) Marsh, K. N.; Brennecke, J. F.; Chirico, R. D.; Frenkel, M.; Heintz, A.; Magee, J. W.; Peters, C. J.; Rebelo, L. P. N.; Seddon, K. R. *Pure Appl. Chem.* **2009**, *81*, 781.

JP102941N